

# Edge of Chaos and Genesis of Turbulence

Abraham C.-L. Chian,<sup>1,2,3,\*</sup> Pablo R. Muñoz,<sup>1,3</sup> and Erico L. Rempel<sup>1,3</sup>

<sup>1</sup>*National Institute for Space Research (INPE) and World Institute for Space Environment Research (WISER),  
P. O. Box 515, São José dos Campos-SP 12227-010, Brazil*

<sup>2</sup>*Observatoire de Paris, LESIA, CNRS, 92195 Meudon, France*

<sup>3</sup>*Institute of Aeronautical Technology (ITA), CTA/ITA/IEFM, São José dos Campos-SP 12228-900, Brazil*  
(Dated: March 8, 2013)

The edge of chaos is analyzed in a spatially extended system, modeled by the regularized long-wave equation, prior to the transition to permanent spatiotemporal chaos. In the presence of coexisting attractors, a chaotic saddle is born at the basin boundary due to a smooth-fractal metamorphosis. As a control parameter is varied, the chaotic transient evolves to well-developed transient turbulence via a cascade of fractal-fractal metamorphoses. The edge state responsible for the edge of chaos and the genesis of turbulence is an unstable travelling wave in the laboratory frame, corresponding to a saddle point lying at the basin boundary in the Fourier space.

*This manuscript was completed on 28 December 2012, and an extended version of this work will be submitted to Physical Review E in 2013.*

There is a growing interest in edge states at the laminar-turbulent boundary which can improve our understanding of the transition from turbulent to laminar flows in fluids and plasmas, as well as the precursors of turbulence [1, 2]. Dynamical systems description of the transition from temporally to spatiotemporally chaotic attractors, based on the regularized long-wave equation (RLWE), provides a simple model to acquire in-depth insights of the laminar-turbulence transition [3, 4]. In this paper we use the RLWE to study the nonlinear dynamics of a spatially extended system prior to the onset of permanent spatiotemporal chaos. The aims are threefold. First, we establish the link between the concept of edge of chaos (EOC) at the boundary of laminar-turbulent transition and the concept of chaotic saddle at the basin boundary of coexisting attractors. Second, we show that a chaotic saddle is born in a smooth-fractal metamorphosis which evolves to well-developed transient turbulence via fractal-fractal metamorphoses. Third, we elucidate the role of the edge state at the basin boundary of coexisting attractors and at the boundary of pseudo basins of coexisting chaotic saddle and attractor before the onset of permanent spatiotemporal chaos, and at the boundary of pseudo basins of coexisting chaotic saddles/attractors after the onset of permanent spatiotemporal chaos.

The driven-damped regularized long-wave equation is given by [3, 4]

$$\partial_t u + c \partial_x u + f u \partial_x u + a \partial_{txx} u = -\nu u - \epsilon \sin(\kappa x - \Omega t) \quad (1)$$

where  $\epsilon$  is the driver amplitude,  $c = 1$ ,  $f = -6$ ,  $a = -0.28711$ ,  $\nu = 0.1$ ,  $\kappa = 1$  and  $\Omega = 0.65$ . We impose periodic boundary conditions  $u(x, t) = u(x + 2\pi, t)$  and solve Eq. (1) numerically using a pseudospectral method by expanding the wave variable  $u(x, t)$  in a Fourier series  $u(x, t) = \sum_{k=-N}^N \hat{u}_k(t) \exp(ikx)$ . We set  $N = 32$  [4]. Since  $u(x, t)$  is a real function, only  $k > 0$  need to be considered, and after dealiasing 20 complex Fourier

modes are kept, thus the phase space has dimension 40. In the absence of driving-dissipation ( $\epsilon = \nu = 0$ ) or when driving-dissipation is relatively weak ( $\epsilon, \nu < 1$ ), Eq. (1) admits a steady wave solution in the form of a solitary traveling wave [5]. If we keep all parameters in Eq. (1) fixed and only vary  $\epsilon$ , the steady wave solution of Eq. (1) eventually becomes unstable and undergoes a diversity of bifurcations, giving rise to a wealth of dynamical phenomena.

At  $\epsilon = 0.199$ , just before the onset of permanent spatiotemporal chaos, the solutions of Eq. (1) exhibit the characteristics of edge of chaos. A technique to detect the edge of chaos is to compute the lifetime of initial conditions in some region of the phase space [1, 2], defined as the time a trajectory takes to converge to the laminar attractor. Figure 1(a) shows the lifetime landscape in a two-dimensional projection of the phase space. The red regions indicate short lifetime, and corresponds to initial conditions whose trajectories do not show the features of transient turbulence (governed by a spatiotemporally chaotic saddle STCS [4]) and converge quickly to the laminar attractor (spatially regular and temporally chaotic attractor). On the other hand, the light blue regions correspond to initial conditions whose temporal evolution displays long chaotic transients before converging to the laminar attractor. The stable manifold of STCS is well approximated by the regions of longer lifetime. The edge of chaos is the boundary dividing the two regions of lifetime in Fig. 1(a).

The cross in Fig. 1(a) marks the position of the edge state (ES), which lies on the edge of chaos. The edge state is found through the bisection method [1]. By integrating many different initial conditions it is seen that the trajectories associated with turbulence have high level of energy bursts; here, energy is defined by  $E = \int_0^{2\pi} [u(x, t)^2 - a u_x(x, t)^2] dx / 4\pi$ . In contrast, the trajectories that converge quickly to the laminar attrac-

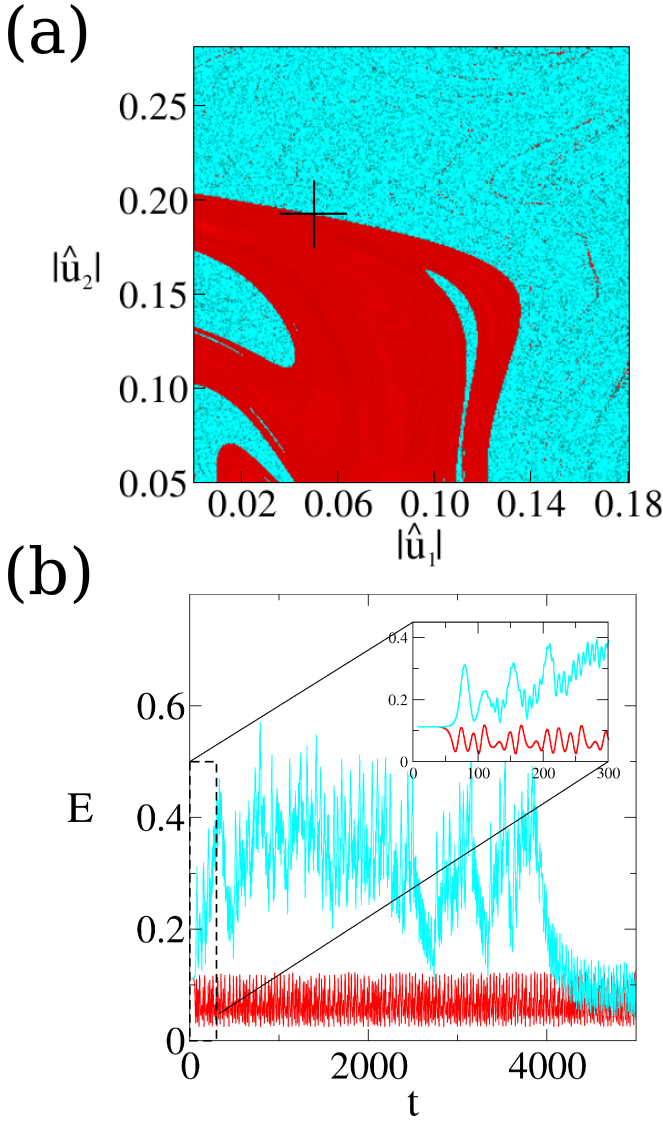


FIG. 1. Edge of chaos is the boundary that separates two regions in the 2D projection of the phase space in (a), at  $\epsilon = 0.199$ , showing the transient lifetime for turbulent trajectories to converge to a laminar attractor. Edge state is indicated by a black cross whose stable manifold is the edge of chaos. The blue (red) regions indicates long (short) lifetimes that correspond to the initial conditions that do (do not) exhibit transient turbulence before converging to a laminar attractor, as illustrated by the time series of energy  $E$  in (b), obtained by the bisection method for two different initial conditions.

tor have low level of energy fluctuations. Beginning with two initial conditions  $u_S$  and  $u_L$ , with short and long lifetimes, respectively, we integrate the condition given by the middle point of the path that connects both conditions,  $u_M = (u_S + u_L)/2$ , until it converges to the laminar attractor. We set the energy level  $E_0 = 0.2$  as a threshold to decide to which region of the phase space  $u_M$  belongs. If the maximum energy along the trajectory of

$u_M$  is lower than  $E_0$ ,  $u_M$  lies in the laminar pseudo-basin and at the next step we set  $u_L = u_M$ . Otherwise,  $u_M$  belongs to the turbulent pseudo-basin, hence at the next step  $u_S = u_M$ . Repeating this procedure, we find pairs of conditions at both sides of the edge of chaos, arbitrarily close to each other. Figure 1(b) shows an example of two initial conditions determined by the bisection method, with the distance between them  $\|u_S - u_L\| < 10^{-12}$ . The red curve is the trajectory of laminar condition  $u_S$ , and the light blue curve is the trajectory of turbulent condition  $u_L$ . As the inset in Fig. 1(b) shows, both trajectories remain close to each other initially with  $E$  remaining almost constant until  $t \sim 50$ . That part of the solutions corresponds to trajectories passing near the stable manifold (EOC) of ES, which is a saddle point in the Fourier space, with constant energy for a given control parameter. For  $t \gtrsim 50$ , the 2 trajectories separate quickly. The laminar trajectory converges immediately to the laminar attractor, while the turbulent trajectory traverses first the vicinity of a chaotic saddle before converging to the laminar attractor at  $t \sim 4000$ . By applying systematically the bisection method it is possible to find a long trajectory close to ES.

At  $\epsilon = 0.199$ , STCS, which is irregular in space and chaotic in time, computed by the stagger-and-step method [6] has a Lyapunov spectrum with 14 positive Lyapunov exponents and a Kaplan-Yorke dimension  $\sim 36$ ; ES is a saddle point, with one positive Lyapunov eigenvalue and 39 negative Lyapunov eigenvalues, whose stable manifold separates the two regions of pseudo-basins in Fig. 1(a); the laminar attractor is spatially regular and temporally chaotic with one positive Lyapunov exponent and a Kaplan-Yorke dimension of  $\sim 22$  [4].

In order to probe the origin of the edge state and the genesis of transient turbulence related to the aforementioned EOC, we construct a detailed bifurcation diagram in Fig. 2 for  $E$  as a function of  $\epsilon$  for attractors, chaotic saddles and ES. We adopt a Poincaré map by plotting a point every time the trajectory obtained from Eq. (1) crosses the plane  $|\hat{u}_2(t)| = 0.1$  with  $d|\hat{u}_2(t)|/dt > 0$ . The chaotic saddle is computed by the sprinkler method [7]. For  $\epsilon = 0$  to  $0.25$  we have identified four different attractors:  $A_1$ ,  $A_2$ ,  $A_3$  and  $A_4$ . In the interval  $\epsilon = 0$  to  $0.079$   $A_1$  is a stable fixed point (thick blue line) with a constant energy for a given  $\epsilon$ , which loses its stability and is converted to a period-1 limit cycle (thin blue line) via a Hopf bifurcation (HB) at  $\epsilon \sim 0.079$ . We observe three small energy jumps in the  $A_1$  branch, one of them is visible in Fig. 2 at  $\epsilon \sim 0.154$ . These jumps represent transitions from one period-1 attractor to another. Although strictly speaking these are different attractors, we refer to them as  $A_1$  along the paper because they occupy roughly the same area in the phase space and their bifurcations do not affect our main analysis. The last period-1 limit cycle vanishes at  $\epsilon \sim 0.1925$ .  $A_2$  appears

via a tangent bifurcation (TB) at  $\epsilon \sim 0.09$  when two fixed points, one stable (thick magenta line) and one unstable (ES, dashed black line), are created. This unstable fixed point corresponds to the edge state that plays a fundamental role in the genesis of transient turbulence and EOC seen in Figs. 1 and 2. At  $\epsilon \sim 0.125$ ,  $A_2$  suffers a Hopf bifurcation and becomes a limit cycle of period-1 (thin magenta line). At  $\epsilon \sim 0.1297$ ,  $A_2$  is bifurcated into a quasiperiodic attractor which loses its stability and vanishes at  $\epsilon \sim 0.13235$ . The coexistence of attractors  $A_1$  and  $A_2$  in the interval  $\epsilon \sim 0.09$  to  $0.13235$  implies the existence of two basins of attraction. We will show that the bifurcation of the basin boundary is responsible for the genesis of transient turbulence. A period-2 attractor  $A_3$  (red line) appears via a saddle-node bifurcation (SNB) at  $\epsilon \sim 0.1774$ , which undergoes a number of different bifurcations as  $\epsilon$  increases, involving a transition to quasiperiodicity, period-doubling cascade, and unstable dimension variability to temporal chaos at  $\epsilon \sim 0.1925$  [8], and at  $\epsilon \sim 0.2$  it loses its stability via an interior crisis (IC) leading to the onset of a spatiotemporally chaotic attractor  $A_4$  (green) [4]. Chian *et al.* [4] demonstrated that for  $\epsilon \lesssim 0.21$   $A_4$  is composed of a spatiotemporally chaotic saddle (STCS, light blue) which preexists as the transient turbulence prior to IC and a temporally chaotic saddle (TCS, grey) evolved from  $A_3$ . TCS turns into a temporally chaotic attractor  $A_3$  at  $\epsilon \sim 0.22105$  due to a boundary crisis (BC). As  $\epsilon$  increases further,  $A_3$  turns into a period-1 limit cycle via an inverse period-doubling cascade and becomes a stable fixed point (thick red line) via a Hopf bifurcation at  $\epsilon \sim 0.2308$ . At  $\epsilon \sim 0.235$ , the stable fixed point  $A_1$  disappears in a tangent bifurcation

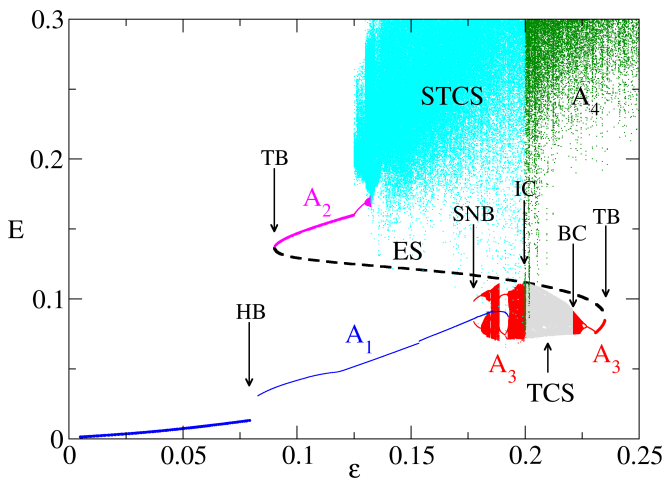


FIG. 2. Bifurcation diagram of  $E$  as a function of  $\epsilon$  for edge state (ES), attractors ( $A_1$ - $A_4$ ), spatiotemporally chaotic saddle (STCS) and temporally chaotic saddle (TCS), showing Hopf bifurcation (HB), tangent bifurcation (TB), saddle-node bifurcation (SNB), interior crisis (IC) and boundary crisis (BC).

(TB), along with ES.  $A_3$  and  $A_4$  coexist for  $\epsilon = 0.22105$  to  $0.2308$ . EOC can be found for  $0.11 \lesssim \epsilon \lesssim 0.2$  where there is coexistence of transient turbulence (STCS), edge state (ES) and spatially regular laminar attractors ( $A_1$ ,  $A_2$ ,  $A_3$ ).

Next we investigate the origin of the edge state and its role in the genesis and evolution of STCS responsible for the transient turbulence. As mentioned earlier, when  $A_2$  appears as a stable fixed point, an unstable fixed point appears simultaneously via TB;  $A_1$  coexists with  $A_2$  for  $0.09 \lesssim \epsilon \lesssim 0.13235$ . The basins of attraction are separated by a boundary. ES is a saddle structure that lies at the basin boundary. We applied the bisection method [1] to detect ES that separates  $A_1$  and  $A_2$ , and discovered that ES is the unstable fixed point born at the tangent bifurcation TB ( $\epsilon \sim 0.09$ ), shown in Fig. 2. The edge state corresponds to an unstable travelling wave moving with the driver speed in the laboratory frame.

Figure 3 shows the basins of attraction of  $A_1$  (blue) and  $A_2$  (magenta) for  $\epsilon = 0.095$ ,  $0.111$ , and  $0.130$ , respectively, along with the edge state (cross). The stable manifold of ES is the basin boundary separating 2 coexisting attractors. For  $\epsilon < \epsilon_M \sim 0.11$ , the basin boundary is smooth as shown by Fig. 3(a) for  $\epsilon = 0.095$ . At  $\epsilon = \epsilon_M$ , a chaotic saddle STCS associated with Smale horseshoe structures is born when the basin boundary becomes fractal as the result of infinite homoclinic crossings between the stable and unstable manifolds of ES due to

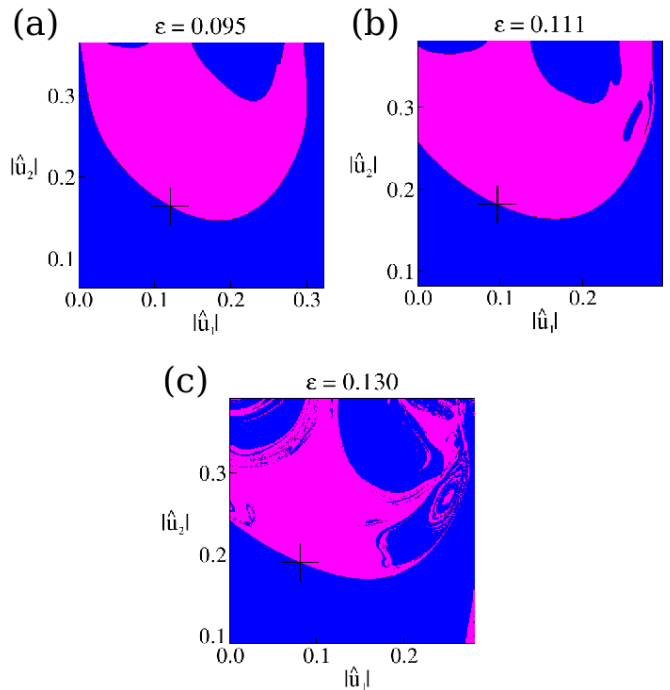


FIG. 3. Basins of attraction for the coexisting attractors  $A_1$  (blue) and  $A_2$  (magenta) at  $\epsilon = 0.095$  (a),  $0.111$  (b),  $0.130$  (c). The black cross denotes the edge state.

a smooth-fractal metamorphosis [9], as seen in Fig. 3(b). As  $\epsilon$  increases for  $\epsilon > \epsilon_M$  the basin boundaries become increasingly complex due to a cascade of fractal-fractal metamorphoses, as shown in Fig. 3(c).

To measure the fractal dimension of the basin boundary for  $0.09 \lesssim \epsilon \lesssim 0.13235$ , where  $A_1$  and  $A_2$  coexist, we compute the uncertainty exponent  $\alpha = D - d$ , where  $D$  is the dimension of the phase space and  $d$  is the fractal dimension of the basin boundary, defined by the uncertainty fraction [10]  $f(\delta) \sim \delta^\alpha$ , where  $\delta$  is the radius of the sphere of uncertainty. The computed  $\alpha$  for this interval is shown by the magenta circles in Fig. 4(a) where we use a two-dimensional phase space projection ( $|\hat{u}_1|, |\hat{u}_2|$ ) with  $D = 2$ . Figure 4(a) shows that for  $\epsilon \lesssim 0.11$   $\alpha$  is  $\approx 1$  implying a smooth basin boundary. For  $\epsilon \gtrsim 0.11$   $\alpha$  becomes  $< 1$  implying a fractal basin boundary. As  $\epsilon$  increases further,  $\alpha$  steadily decreases implying the occurrence of a cascade of fractal-fractal metamorphoses [9], in agreement with changes in the basin boundaries seen in Fig. 3.

By noticing that the structure of the basins of attraction of  $A_1$  and  $A_2$  just before the disappearance of  $A_2$  is very similar to the lifetime function for  $A_1$  just after the disappearance of  $A_2$  in the same region of the phase space, we use this information to compute the fractal dimension of the pseudo-basin boundary for  $0.14 \leq \epsilon \leq 0.19$ . We define the lifetime difference for 2 initial conditions separated by  $\delta$  as  $\Delta T(r) = |T(r + \delta) - T(r)|$ , where  $T(r)$  is the time an initial condition  $r$  takes to converge to  $A_1$ . We classify an initial condition  $r$  as uncertain if  $\Delta T(r) > \Delta_{th}$ , where  $\Delta_{th}$  is the time-difference threshold. The uncertainty exponent for each  $\Delta_{th}$  is given by the slope of the line fitted by a linear regression. The values of  $f(\delta)$  calculated for the interval (ii) are indicated by the blue squares in Fig. 4(a).

To compute the fractal dimension of the pseudo-basin boundary for  $\epsilon = 0.199$ , we use the expression for the upper bound of the uncertainty exponent as a function of the mean lifetime of the chaotic saddle  $\tau$  [4, 9] and the maximum Lyapunov exponent  $\lambda_{max}$ ,  $\alpha \leq 1/(\tau\lambda_{max})$  [11]. Chian *et al.* [4] accurately obtained  $\lambda_{max} = 0.1405$  and  $\tau = 353.3$  (in units of the driver period) for  $\epsilon = 0.199$ , thus  $\alpha$  calculated from the upper bound formula is 0.002018, denoted by the green triangle in Fig. 4(a).

To quantify the degree of spatial disorder of the chaotic saddle created at  $\epsilon \gtrsim 0.11$ , we compute the time-average of the Fourier power spectral Shannon entropy [4] of STCS, given by  $S_A(t) = -\sum_{k=1}^N p_k(t) \ln p_k(t)$ , where  $p_k(t) = |\hat{u}_k(t)|^2 / \sum_{k=1}^N |\hat{u}_k(t)|^2$ . Figure 4(a) shows that the degree of spatial disorder increases with  $\epsilon$  until it reaches the maximum value near  $\epsilon \sim 0.199$ .

The increase of the degree of spatial disorder with increasing driver amplitude is accompanied by an increase of temporal chaos. A way to estimate the number of positive Lyapunov exponents is to compute a large num-

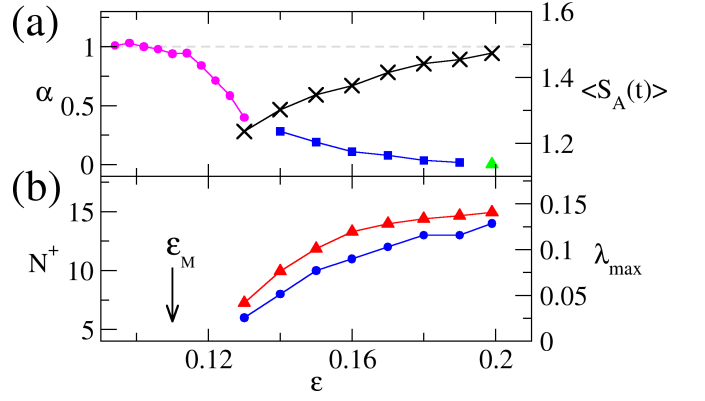


FIG. 4. Variation with  $\epsilon$  of: a) the uncertainty exponent  $\alpha$  (magenta circles, blue squares, green triangle) and the time-average power spectral entropy  $\langle S_A(t) \rangle$  (cross), b) the number of positive Lyapunov exponents  $N^+$  (blue circles) and the maximum Lyapunov exponent  $\lambda_{max}$  (red triangles).  $\epsilon_M$  indicates the genesis of a chaotic saddle (STSC).

ber of finite-time Lyapunov spectra of STCS and taking the average [12]. Figure 4(b) shows that the number of positive Lyapunov exponents  $N^+$  (blue circles) increases steadily with increasing  $\epsilon$ , reaching its maximum value of  $N^+ = 14$  at  $\epsilon \sim 0.199$ . Similar behavior is observed for the maximum Lyapunov exponent  $\lambda_{max}$  (red triangle), shown in Fig. 4(b). Figure 4 provides a consistent overview of the genesis and evolution of the transient turbulence showing that the degree of complexity of transient turbulence (STCS) increases as  $\epsilon$  increases and evolves to a well-developed transient turbulence before the transition to permanent spatiotemporal chaos.

In conclusion, we have demonstrated that prior to the onset of permanent spatiotemporal chaos the regularized long-wave equation exhibits the behavior of edge of chaos (EOC), whereby a trajectory traverses a transient turbulent state before converging to a laminar state. The edge state responsible for the EOC and the genesis of turbulence was identified and a sequence of metamorphoses of the EOC was shown to be responsible for the appearance of a chaotic saddle and its subsequent evolution to a well-developed transient turbulence. Our results provide a much clearer picture of the origin of turbulence in the regularized long-wave equation, which has been extensively studied as a general model of transition to spatiotemporal chaos [3–5, 8].

This work is supported by CAPES, CNPq and FAPESP. A.C.L.C. thanks the award of a Marie Curie International Incoming Fellowship and the hospitality of Paris Observatory.

\* abraham.chian@gmail.com

- [1] J. D. Skufca, J. A. Yorke, and B. Eckhardt, Phys. Rev. Lett. **96**, 174101 (2006).
- [2] T. M. Schneider, B. Eckhardt, and J. A. Yorke, Phys. Rev. Lett. **99**, 034502 (2007); L. van Veen and G. Kawahara, *ibid.* **107**, 114501 (2011); A. de Lozar, F. Mellibovsky, M. Avila, and B. Hof, *ibid.* **108**, 214502 (2012); S. Cherubini, P. De Palma, J. C. Robinet, and A. Bottaro, Phys. Fluids **23**, 051705 (2011).
- [3] K. He and A. C.-L. Chian, Phys. Rev. Lett. **91**, 034102 (2003).
- [4] E. L. Rempel and A. Chian, Phys. Rev. Lett. **98**, 014101 (2007); A. C.-L. Chian, R. A. Miranda, E. L. Rempel, Y. Saiki, and M. Yamada, *ibid.* **104**, 254102 (2010).
- [5] K. He and A. Salat, Phys. Lett. A **132**, 175 (1988).
- [6] D. Sweet, H. E. Nusse, and J. A. Yorke, Phys. Rev. Lett. **86**, 2261 (2001).
- [7] H. Kantz and P. Grassberger, Physica D **17**, 75 (1985); G.-H. Hsu, E. Ott, and C. Grebogi, Phys. Lett. A **127**, 199 (1988).
- [8] P. P. Galuzio, S. R. Lopes, and R. L. Viana, Phys. Rev. Lett. **105**, 055001 (2010); Phys. Rev. E **84**, 056211 (2011).
- [9] C. Grebogi, E. Ott, and J. A. Yorke, Phys. Rev. Lett. **56**, 1011 (1986); C. Grebogi, E. Ott, and J. A. Yorke, Physica D **24**, 243 (1987); Y. Lai and T. Tél, *Transient Chaos - Complex Dynamics on Finite-Time Scales* (Springer, 2011).
- [10] C. Grebogi, S. W. McDonald, E. Ott, and J. A. Yorke, Phys. Lett. A **99**, 415 (1983); F. C. Moon and G.-X. Li, Phys. Rev. Lett. **55**, 1439 (1985).
- [11] T. Tél, in *Experimental Study And Characterization Of Chaos*, edited by B.-L. Hao (World Scientific, 1990) pp. 149–211; V. Paar and N. Pavin, Mod. Phys. Lett. B **14**, 167 (2000).
- [12] E. Ott, *Chaos in dynamical systems* (Cambridge University Press, 1993).